

## LETTER TO THE EDITOR OPEN

Cryo-EM structure of constitutively active human Frizzled 7 in complex with heterotrimeric G<sub>s</sub>

© The Author(s) 2021

Cell Research (2021) 31:1311–1314; https://doi.org/10.1038/s41422-021-00525-6

Dear Editor,

The ten mammalian Frizzleds (FZD<sub>1–10</sub>) belong to the class F of G protein-coupled receptors (GPCRs) and mediate WNT signaling through interaction with transducer proteins including Dishevelled (DVL) or heterotrimeric G proteins.<sup>1</sup> Their involvement in human disease has put FZDs at the forefront of drug targets, especially anti-cancer therapy.<sup>2</sup> However, no drugs have been developed for efficient pharmacological modulation of FZDs, partially owing to the limited understanding of FZD structure and activation mechanisms.<sup>1,3</sup> Among class F, FZD<sub>7</sub> is intensively pursued due to its relevance in various tumor models, particularly in intestinal cancers.<sup>4</sup> Detailed structures of the receptor complexes would allow for structure-guided discovery of new drug candidates. FZD<sub>1–10</sub> share structural similarity with the related class F member Smoothed (SMO), which mediates Hedgehog signaling and is a validated target for cancer therapy.<sup>2</sup> In an effort to understand the structural basis of FZD activation and transducer interaction, we solved the structure of human FZD<sub>7</sub> in complex with heterotrimeric mini G<sub>s</sub> (mG<sub>s</sub>).<sup>5</sup>

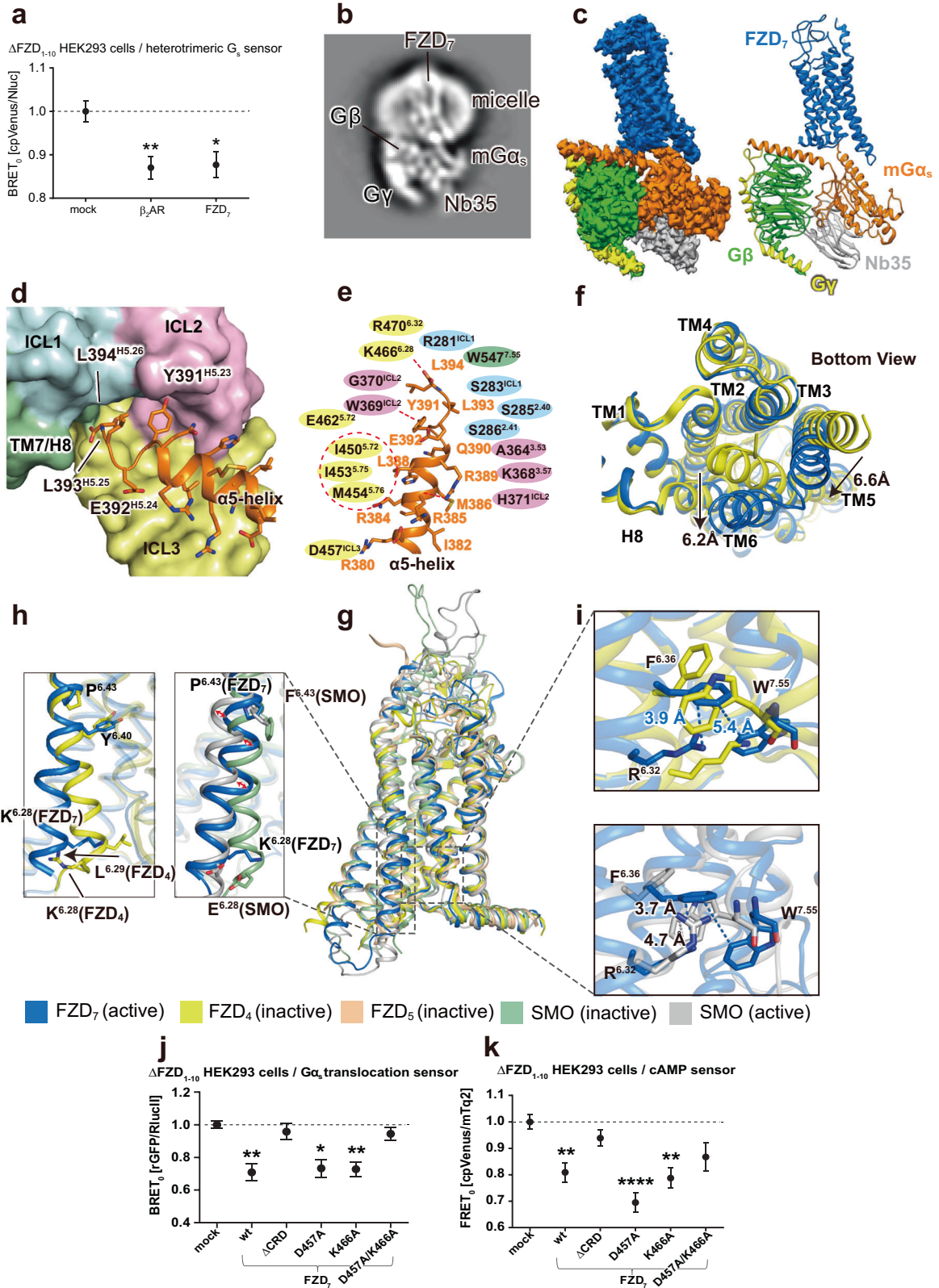
Based on the evidence that FZD<sub>7</sub> interacts with G<sub>s</sub> to mediate muscle hypertrophy,<sup>6,7</sup> we assessed its ability to activate heterotrimeric G<sub>s</sub> independently of WNT stimulation. Co-expression of FZD<sub>7</sub> with a bioluminescence resonance energy transfer (BRET)-based G<sub>s</sub> biosensor,<sup>8</sup> reporting the rearrangement or dissociation of G<sub>α<sub>s</sub></sub> and G<sub>βγ</sub> following receptor engagement and G protein activation, revealed that FZD<sub>7</sub> exhibits constitutive activity similar to the class A β<sub>2</sub>-adrenoceptor (Fig. 1a; Supplementary information, Fig. S1a, b). Using an analogous assay that measures activity-dependent G<sub>α<sub>s</sub></sub> translocation (Supplementary information, Fig. S1c), we found that the constitutive activity of FZD<sub>7</sub> correlates with increased receptor expression (Supplementary information, Fig. S1d, e). Given the robust constitutive activity of FZD<sub>7</sub> towards G<sub>s</sub>, we reconstituted purified, full-length human FZD<sub>7</sub>, heterotrimeric mG<sub>s</sub> and Nanobody35 (Nb35), which stabilizes the nucleotide-free G<sub>α<sub>s</sub></sub> and G<sub>β</sub> subunits,<sup>9</sup> in the absence of ligand and obtained pure complexes following size exclusion chromatography (Supplementary information, Fig. S2). The final complex was composed of FZD<sub>7</sub>, mG<sub>α<sub>s</sub></sub>, G<sub>β</sub>, G<sub>γ</sub> and Nb35, which could be clearly identified by 2D classification (Fig. 1b; Supplementary information, Fig. S2d). We used single-particle cryo-EM analysis to determine the 3D structure of this complex. After several rounds of classification and auto-refinement, the resolution of the final structure reached 3.2 Å allowing us to build an atomic model based on the density map (Fig. 1c; Supplementary information, Figs. S3–S5, Table S1).

In accordance with the functional evidence for constitutive activity, the FZD<sub>7</sub>–mG<sub>s</sub> complex structure provides the structural basis for ligand-independent G protein coupling (Fig. 1c). The interface between FZD<sub>7</sub> and mG<sub>s</sub> is dominated by the distal C-terminal segment of the α5-helix in mG<sub>α<sub>s</sub></sub> (Fig. 1d, e). The C-terminal

leucine residues (L393<sup>H5.25</sup>, L394<sup>H5.26</sup>; superscripts refer to the residue position in the common G<sub>α</sub> numbering scheme for G proteins/GPCRdb) are inserted into the helical bundle of the receptor. L393<sup>H5.25</sup> and L394<sup>H5.26</sup> establish extensive interactions with FZD<sub>7</sub> residues yielding a locally converged network that stabilizes the complex (Fig. 1e). The terminal carboxyl group of L394<sup>H5.26</sup> in mG<sub>α<sub>s</sub></sub> forms an ionic bond with K466<sup>6.28</sup>, and residues R281<sup>1CL1</sup>, K552<sup>8.49</sup> and R470<sup>6.32</sup> of FZD<sub>7</sub> are located in close proximity (superscript numbers refer to the Ballesteros and Weinstein numbering system). Y391<sup>H5.23</sup> forms a hydrogen bond with the backbone of W369<sup>1CL2</sup>. Residues I450<sup>5.72</sup>, I453<sup>5.75</sup> and M454<sup>5.76</sup> of FZD<sub>7</sub> form a hydrophobic cleft accommodating L388<sup>H5.20</sup>. Furthermore, R385<sup>H5.17</sup> forms an ionic bond with D457 in ICL3, further strengthening the interaction between the α5-helix and FZD<sub>7</sub>. In summary, the recognition of G<sub>α<sub>s</sub></sub> by FZD<sub>7</sub> is primarily governed by a network of hydrogen bonding and electrostatic interactions contributed from the C-terminal segment of the α5-helix (D381<sup>H5.13</sup>–L394<sup>H5.26</sup>), among which, interactions with L394<sup>H5.26</sup> lock the α5-helix tail in an uncoiled, elongated conformation (Fig. 1e).

The placement of the α5-helix of mG<sub>α<sub>s</sub></sub> in the core of FZD<sub>7</sub> stabilizes an open FZD<sub>7</sub> conformation. We compared the FZD<sub>7</sub>–mG<sub>s</sub> structure with the available inactive-state FZD<sub>4</sub> crystal structure (PDB: 6BD4) and the inactive-state FZD<sub>5</sub> cryo-EM structure (PDB: 6WW2) and observed a clear outward bending of TM6 and an inward shift of TM5 at the cytoplasmic side (Fig. 1f–h)—a conformational change characteristic of active-state class A and B GPCRs. This helical rearrangement is achieved through interaction of TM6 and TM5 with mG<sub>s</sub> and opening of the molecular switch between TM6 and TM7 (R<sup>6.32</sup>/W<sup>7.55</sup>; Fig. 1i).<sup>7</sup> Comparing inactive FZD<sub>4</sub> with FZD<sub>7</sub>–mG<sub>s</sub> reveals that the extracellular portion of TM6 of FZD<sub>7</sub> extends above the surface of the lipid bilayer at an angle of 45° (Supplementary information, Figs. S6, S7), similar to what we have predicted in previous models<sup>10</sup> and in contrast to the almost 90° bending in the FZD<sub>4</sub> structure.<sup>11</sup> Moreover, conserved cysteines within the hinge domain form disulfide bonds to both stabilize its structure and to link it with ECL1 (C210–C230; C234–C315<sup>ECL1</sup>) (Supplementary information, Fig. S6).<sup>12</sup>

To better understand the activation mechanism of FZD<sub>7</sub> and G protein coupling to class F receptors, we compared the FZD<sub>7</sub>–mG<sub>s</sub> structure with the agonist (24(S), 25-epoxycholesterol)-bound structure of SMO–G<sub>i</sub><sup>13</sup> (PDB: 6OT0). The helical arrangement at the upper portion of the FZD<sub>7</sub> transmembrane core is more compact, presumably due to the absence of ligand (Supplementary information, Fig. S7). At the lower portion of TM6, substantially distinct conformations are observed between the SMO–G<sub>i</sub> and FZD<sub>7</sub>–mG<sub>s</sub> structures. Most strikingly, TM6 in SMO–G<sub>i</sub> undergoes a parallel outward movement compared to inactive SMO, whereas TM6 in the FZD<sub>7</sub>–mG<sub>s</sub> complex accomplishes a



similar displacement of the cytoplasmic portion through a kink in the helix (Fig. 1h). The ionic interactions between TM6, ICL3 and the  $\alpha 5$ -helix of mG $\alpha_s$  (K466<sup>6.28</sup>-L394<sup>H5.26</sup> and D457-R385<sup>H5.17</sup>) are likely to be the main contributors in maintaining this kink. In addition, Y478<sup>6.40</sup> forms  $\pi$ - $\pi$  interaction with W354<sup>3.43</sup> to further

maintain the bent TM6 conformation (Supplementary information, Fig. S7).

While the most evident structural rearrangements relate to TM6, additional positional shifts of TM2, TM3, TM4 and TM5 in the FZD<sub>7</sub>-mG $\alpha_s$  complex are observed when compared to the SMO-G $\alpha_s$

**Fig. 1 Structure of constitutively active FZD<sub>7</sub> in complex with heterotrimeric mG<sub>s</sub>.** **a** Normalized BRET<sub>0</sub> values of  $\Delta$ FZD<sub>1-10</sub> HEK293 cells transiently co-transfected with the G<sub>s</sub> BRET sensor along with either negative control (mock), the  $\beta_2$ -adrenoceptor ( $\beta_2$ AR) or FZD<sub>7</sub>. Data are represented as the means  $\pm$  SEM of raw BRET<sub>0</sub> that were obtained from simple linear regression of five independent experiments measured in quadruplicates shown in Supplementary information, Fig. S1A and normalized to the negative control. \* $P$  < 0.05; \*\* $P$  < 0.01 (one-way ANOVA followed by Sidak's multiple comparison). **b** An annotated 2D class average of FZD<sub>7</sub>-mG<sub>s</sub>-Nb35 complex. **c** Overall density map and atomic model of FZD<sub>7</sub>-mG<sub>s</sub>-Nb35 complex (CRD was omitted due to linker flexibility). FZD<sub>7</sub>, blue; mG $\alpha_s$ , orange; G $\beta$ , green; G $\gamma$ , yellow; Nb35, gray. **d** Insertion of the  $\alpha$ 5-helix (mG $\alpha_s$ , orange) into FZD<sub>7</sub> helical bundle represented as surface (ICL1, blue; ICL2, pink; ICL3, yellow; TM7/H8, green). **e** Schematics of interactions between FZD<sub>7</sub> and  $\alpha$ 5-helix. Hydrogen bonds are shown as red dashed lines. The red circle represents the hydrophobic interaction network. Yellow shades indicate residues that reside in TM5/6/ICL3; pink, TM3/4/ICL2; blue, TM1/2/ICL1; green, TM7/H8. **f** Superposition of FZD<sub>7</sub> (blue) and FZD<sub>4</sub> (yellow) structures, viewed from the intracellular side (bottom view). **g** Superposition of the active FZD<sub>7</sub> structure (blue) with the inactive FZD<sub>4</sub> (PDB: 6BD4, yellow), inactive FZD<sub>5</sub> (PDB: 6WW2, light pink), active SMO (PDB: 6OT0, gray) and inactive SMO (PDB: 5V57, green) structures. **h** Comparison of the cytoplasmic portion of TM6 (from K<sup>6.28</sup> to P<sup>6.43</sup>) in FZD<sub>7</sub>, FZD<sub>4</sub>, active SMO and inactive SMO structures. **i** R<sup>6.32</sup>, F<sup>6.36</sup>, W<sup>7.55</sup> network in FZD<sub>7</sub>, FZD<sub>4</sub> and active SMO structures. Blue dashed lines indicate the distance of F<sup>6.36</sup>-W<sup>7.55</sup> and F<sup>6.36</sup>-R<sup>6.32</sup> in FZD<sub>7</sub>. Gray dashed lines indicate the distance of R<sup>6.32</sup>-W<sup>7.55</sup> and W<sup>7.55</sup>-F<sup>6.36</sup> in active SMO structure. **j** Normalized BRET<sub>0</sub> values of  $\Delta$ FZD<sub>1-10</sub> HEK293 cells transiently co-transfected with rGFP-CAAX and G $\alpha_s$ -67-RlucII, along with either negative control (mock), wild-type FZD<sub>7</sub>,  $\Delta$ CRD-FZD<sub>7</sub> or the indicated FZD<sub>7</sub> mutants. Data are represented as the means  $\pm$  SEM of raw BRET<sub>0</sub> that were obtained from simple linear regression of four independent experiments measured in quadruplicates shown in Supplementary information, Fig. S11b and normalized to the negative control. \*\* $P$  < 0.01; \*\*\* $P$  < 0.001 (one-way ANOVA followed by Tukey's multiple comparison). **k** Normalized FRET<sub>0</sub> values of  $\Delta$ FZD<sub>1-10</sub> HEK293 cells transiently co-transfected with the FRET-based cAMP biosensor along with either negative control (mock), wild-type FZD<sub>7</sub>,  $\Delta$ CRD-FZD<sub>7</sub> or the indicated FZD<sub>7</sub> mutants. Data are represented as the means  $\pm$  SEM of raw FRET<sub>0</sub> that were obtained from simple linear regression of five independent experiments measured in quadruplicates shown in Supplementary information, Fig. S11c and normalized to the negative control. \*\* $P$  < 0.01; \*\*\*\* $P$  < 0.0001 (one-way ANOVA followed by Sidak's multiple comparison).

complex. These four helices constitute a more compact bundle in the FZD<sub>7</sub>-mG<sub>s</sub> structure, partially stabilized by a network of  $\pi$  interactions (Supplementary information, Fig. S7e). In a cooperative manner, these interactions promote the cytoplasmic portion of TM4 shifting inward by  $\sim$ 2 Å (comparing the Ca of L383<sup>4,47</sup> in FZD<sub>7</sub>-mG<sub>s</sub> with corresponding L362<sup>4,47</sup> in SMO-G<sub>i</sub> complex structures) (Supplementary information, Fig. S7f, black arrow).

A conserved molecular switch between TM6 and TM7 was previously identified for all class F GPCRs, maintaining the receptor in an inactive conformation (observed as a hydrogen-bonding distance between R<sup>6.32</sup> and the backbone of W<sup>7.55</sup>) in all inactive class F receptor structures.<sup>7</sup> The polar interactions between R<sup>6.32</sup> and W<sup>7.55</sup> are broken in active SMO-G<sub>i</sub> and the FZD<sub>7</sub>-mG<sub>s</sub> complexes, resulting in a 6.4 Å distance between R470<sup>6.32</sup> and W547<sup>7.55</sup> in the FZD<sub>7</sub>-mG<sub>s</sub> complex (Fig. 1f, h).<sup>7</sup>

To explore the conformational dynamics around the open and active FZD<sub>7</sub> structure, we performed molecular dynamics (MD) simulations of FZD<sub>7</sub> in complex with mG<sub>s</sub>393<sup>5</sup> (Supplementary information, Fig. S8). Monomeric mG<sub>s</sub> facilitated MD simulations due to its small size while minimizing the effect on receptor dynamics. These MD simulations allowed us to monitor general receptor integrity and the status of the molecular switch by assessing the angle of the kinked TM6 and the distance between R470<sup>6.32</sup> and W547<sup>7.55</sup>. The overall hallmark of FZD<sub>7</sub> activation — the kink in TM6 — is maintained over the time course of the simulation (measured as an angle between the backbone nitrogen atoms of V485<sup>6.47</sup>, P481<sup>6.43</sup> and E462<sup>6.24</sup>). P<sup>6.43</sup> is fully conserved among the FZD paralogues, but not in SMO (F<sup>6.43</sup>) (Supplementary information, Fig. S9). Analogous to P<sup>6.50</sup> and P<sup>6.47</sup> in class A and B receptors, respectively (Supplementary information, Fig. S10), P481<sup>6.43</sup> is likely to contribute to the observed outward movement of the lower part of TM6<sup>14</sup> (Fig. 1f, h). In the MD trajectories, the conformational changes of TM6 are manifested by the disruption of the molecular switch and a rearrangement of an extended aromatic network stabilizing the active receptor conformation (Supplementary information, Fig. S8). R470<sup>6.32</sup> and the backbone oxygen atom of W547<sup>7.55</sup> remain at over 8 Å distance throughout the simulation, rendering hydrogen bonding impossible between these two residues. Instead, R470<sup>6.32</sup> is frequently bound with the carboxyl terminus of L<sup>H5.26</sup> of mG $\alpha_s$ . Interestingly, R470<sup>6.32</sup> remains within hydrogen-bonding distance to the carboxyl terminus of L<sup>H5.26</sup> more often than K466<sup>6.28</sup>, indicating that these positively charged residues lock the carboxyl tail between them

(Supplementary information, Fig. S8d). This could contribute to the observed non-helical conformation of the tail of the  $\alpha$ 5-helix.

To gather functional evidence for the FZD<sub>7</sub>-mG<sub>s</sub> interface and its role in maintaining the constitutive activity of FZD<sub>7</sub> towards G<sub>s</sub>, we employed a mutagenesis-based approach in combination with assessment of G $\alpha_s$  translocation and cAMP production as functional readouts of G<sub>s</sub>-dependent signaling. We focused on D457 (in ICL3) and K466<sup>6.28</sup>, which interact with the  $\alpha$ 5-helix of mG $\alpha_s$ . Mutating either D457 or K466<sup>6.28</sup> to alanine alone did not affect the constitutive activity of FZD<sub>7</sub> on G<sub>s</sub> translocation or cAMP production (Fig. 1j, k; Supplementary information, Figs. S11, S12). However, the double mutant D457A/K466<sup>6.28</sup>A abrogated FZD<sub>7</sub> constitutive activity towards G<sub>s</sub>, suggesting that these mutations collectively interfere with G protein coupling. In contrast, the double mutant did not affect the ability of FZD<sub>7</sub> to mediate WNT-induced activation of the WNT/ $\beta$ -catenin pathway as assessed by the TOPFlash reporter assay (Supplementary information, Fig. S13), underlining the concept of conformational selection for DVL-dependent signaling over G protein coupling as has been suggested previously.<sup>7,15</sup>

Although the CRD could not be resolved in the present structure, we observed that removal of the CRD ( $\Delta$ CRD-FZD<sub>7</sub>) resulted in the inability to reconstitute the receptor-mG<sub>s</sub> complex in vitro to the same extent as that of full-length FZD<sub>7</sub> (Supplementary information, Fig. S14). Thus, we surmised that the CRD is required for FZD<sub>7</sub>-mG<sub>s</sub> complex stability and that removal of the CRD could decrease constitutive activity. Therefore, we assessed the ability of the  $\Delta$ CRD-FZD<sub>7</sub> construct to functionally couple to G<sub>s</sub> by assessing G $\alpha_s$  translocation and cAMP production (Fig. 1j, k). Removal of the CRD blunted the constitutive activity towards G<sub>s</sub> signaling as evidenced by the lack of G $\alpha_s$  translocation and cAMP production. These data underline the requirement for the CRD to maintain constitutive activity of FZD<sub>7</sub> towards heterotrimeric G proteins through intramolecular allostery.

In conclusion, we report the cryo-EM structure of FZD<sub>7</sub>-mG<sub>s</sub> demonstrating how constitutive activity feeds into downstream signaling via heterotrimeric G proteins. With respect to the overall diversity among GPCRs, FZD<sub>7</sub> has evolved a unique way to maintain certain homologous movements consistent with class A and B GPCR activation, while adapting its class-specific architecture to mediate G protein activation. While the classical hallmarks of G protein engagement are present in our structure, several differences can be found at the interface between the receptor and the G protein suggesting that FZDs harbor their own



selectivity determinants for heterotrimeric G proteins. In short, the present structure of constitutively active FZD<sub>7</sub>-mG<sub>s</sub>, alongside previously published inactive structures of FZD<sub>4</sub> and FZD<sub>5</sub>, opens the door to more accurate modeling of other FZDs and a platform for in silico drug discovery, which will aid in the discovery of new treatments to help those afflicted with diseases of WNT-FZD signaling.

Lu Xu<sup>1,2,3,4,9</sup>, Bo Chen<sup>1,9</sup>, Hannes Schihada<sup>5,9</sup>,  
Shane C. Wright<sup>5,6,9</sup>, Ainoleena Turku<sup>5,8</sup>, Yiran Wu<sup>1</sup>,  
Gye-Won Han<sup>7</sup>, Maria Kowalski-Jahn<sup>5</sup>, Pawel Kozielowicz<sup>5</sup>,  
Carl-Fredrik Bowin<sup>5</sup>, Xianjun Zhang<sup>1,2,3,4,7</sup>, Chao Li<sup>1,2,3,4</sup>,  
Michel Bouvier<sup>6</sup>, Gunnar Schulte<sup>5,8</sup> and Fei Xu<sup>1,2,3,4</sup>✉  
<sup>1</sup>iHuman Institute, ShanghaiTech University, Shanghai, China.  
<sup>2</sup>School of Life Science and Technology, ShanghaiTech University, Shanghai, China. <sup>3</sup>Center for Excellence in Molecular Cell Science, Shanghai Institutes for Biological Sciences, Chinese Academy of Sciences, Shanghai, China. <sup>4</sup>University of Chinese Academy of Sciences, Beijing, China. <sup>5</sup>Section of Receptor Biology & Signaling, Department of Physiology & Pharmacology, Karolinska Institutet, Stockholm, Sweden. <sup>6</sup>Institute for Research in Immunology and Cancer, Department of Biochemistry and Molecular Medicine, Université de Montréal, Montréal, QC, Canada. <sup>7</sup>Departments of Biological Sciences and Chemistry, Bridge Institute, University of Southern California, Los Angeles, CA, USA. <sup>8</sup>Present address: Orion Pharma R&D, Espoo, Finland. <sup>9</sup>These authors contributed equally: Lu Xu, Bo Chen, Hannes Schihada, Shane C. Wright  
✉email: [gunnar.schulte@ki.se](mailto:gunnar.schulte@ki.se); [xufei@shanghaitech.edu.cn](mailto:xufei@shanghaitech.edu.cn)

## DATA AVAILABILITY

The cryo-EM 3D map of the FZD<sub>7</sub>-mG<sub>s</sub>-Nb35 complex has been deposited in EMD database with accession code EMD-31340; the coordinates have been deposited in PDB database with accession code 7EVW. The MD simulation data is available at [www.gpcrmd.org](http://www.gpcrmd.org) with ID 245.

## REFERENCES

- Schulte, G. & Wright, S.C. *Trends Pharmacol. Sci.* **39**, 828–842 (2018).
- Taipale, J. & Beachy, P.A. *Nature* **411**, 349–54 (2001).
- Kozielowicz, P., Turku, A. & Schulte, G. *Mol. Pharmacol.* **97**, 62–71 (2020).
- Pheesse, T., Flanagan, D. & Vincan, E. *Cancers* **8**, <https://doi.org/10.3390/cancers8050050> (2016).
- Nehmé, R., Carpenter, B., Singhal, A., Strege, A., Edwards, P.C. & White, C.F. *PLoS ONE* **12**, e0175642 (2017).
- von Maltzahn, J., Bentzinger, C.F. & Rudnicki, M.A. *Nat. Cell. Biol.* **14**, 186–91 (2012).
- Wright, S.C., Kozielowicz, P., Kowalski-Jahn, M., Petersen, J., Bowin, C.F. & Slodkowicz, G. et al. *Nat. Commun.* **10**, 667 (2019).
- Schihada, H., Shekhani, R. & Schulte, G. *bioRxiv* <https://doi.org/10.1101/2021.02.05.429900> (2021).
- Rasmussen, S.G. et al. *Nature* **477**, 549–55 (2011).
- Kozielowicz, P. et al. *Nat. Commun.* **11**, 414 (2020).
- Yang, S. et al. *Nature* **560**, 666–70 (2018).
- Valnohova, J., Kowalski-Jahn, M., Sunahara, R.K. & Schulte, G. *J. Biol. Chem.* **293**, 17875–87 (2018).
- Qi, X. et al. *Nature* **571**, 279–83 (2019).
- Turku, A., Schihada, H., Kozielowicz, P., Bowin, C.F. & Schulte, G. *Nat. Commun.* <https://doi.org/10.1038/s41467-021-24004-z> (2021).
- Bowin, C.F., Inoue, A. & Schulte, G. *J. Biol. Chem.* **294**, 11677–84 (2019).

## ACKNOWLEDGEMENTS

This work was supported by the National Key R&D Program of China (2018YFA0507000 to F.X.), and the National Natural Science Foundation of China (32071194 to F.X.). Work at Karolinska Institutet was supported by Karolinska Institutet, the Swedish Research Council (2017-04676; 2019-01190), the Swedish Cancer Society (CAN2017/561, 20 1102 PjF, 20 0264P), the Novo Nordisk Foundation (NNF17OC0026940; NNF20OC0063168), The Swedish Society of Medical Research (SSMF; P19-0055), the Lars Hierta Memorial Foundation (FO2019-0086, FO2020-0304), The Alex and Eva Wallström Foundation for Scientific Research and Education (2020-00228), and the German Research Foundation (DFG, 427840891; KO 5463/1-1). S.C.W. is supported by a fellowship from the Swedish Society for Medical Research (P18-0098). Computational resources were provided by the Swedish National Infrastructure for Computing (SNIC 2020/5-500). M.B. is funded by the CIHR (FDN-148431) and holds a Canada Research Chair in Signal Transduction and Molecular Pharmacology. We thank Qiwen Tan, Lu Zhang, Junlin Liu, Na Chen, Qiaoyun Shi and Wei Xiao from iHuman Institute for protein cloning and expression support; Qianqian Sun, Yunhun Liu and Zhihui Zhang at the Bio-EM facility at ShanghaiTech University for technical support on data collection. We thank Vadim Cherezov from University of Southern California for advice on structure refinement.

## AUTHOR CONTRIBUTIONS

L.X. performed cloning, protein purification, cryo-EM sample preparation, data collection and structure analysis; B.C. performed cryo-EM data processing, model building and refinement; Y.W. assisted with the structure analysis and some calculations; G.W.H. was responsible for structure quality control; X.Z. and C.L. characterized the protein expression at early phase of the project; H.S. and S.C.W. performed functional biosensor experiments; M.K.J. and P.K. performed FZD<sub>7</sub> construct mutagenesis for functional analysis; C.F.B. validated FZD<sub>7</sub> surface expression; A.T. performed the MD simulation and analysis and contributed to model interpretation and visualization. F.X. conceived the project. F.X. and G.S. designed, coordinated and supervised the experiments. L.X., B.C., S.C.W., H.S., M.B., G.S. and F.X. wrote the manuscript.

## COMPETING INTERESTS

M.B. is the president of the scientific advisory board for Domain Therapeutics. M.B. has filed patent applications related to some of the biosensors used in this work and the technology has been licensed to Domain Therapeutics.

## ADDITIONAL INFORMATION

**Supplementary information** The online version contains supplementary material available at <https://doi.org/10.1038/s41422-021-00525-6>.

**Correspondence** and requests for materials should be addressed to G.S. or F.X.

**Reprints and permission information** is available at <http://www.nature.com/reprints>



**Open Access** This article is licensed under a Creative Commons Attribution 4.0 International License, which permits use, sharing, adaptation, distribution and reproduction in any medium or format, as long as you give appropriate credit to the original author(s) and the source, provide a link to the Creative Commons license, and indicate if changes were made. The images or other third party material in this article are included in the article's Creative Commons license, unless indicated otherwise in a credit line to the material. If material is not included in the article's Creative Commons license and your intended use is not permitted by statutory regulation or exceeds the permitted use, you will need to obtain permission directly from the copyright holder. To view a copy of this license, visit <http://creativecommons.org/licenses/by/4.0/>.

© The Author(s) 2021